

1 LEVERAGING MULTI-MESSENGER ASTROPHYSICS FOR DARK MATTER SEARCHES

By

Daniel Nicholas Salazar-Gallegos

A DISSERTATION

Submitted to  
Michigan State University  
in partial fulfillment of the requirements  
for the degree of

Physics—Doctor of Philosophy  
Computational Mathematics in Science and Engineering—Dual Major

Today

**ABSTRACT**

3 I did Dark Matter with HAWC and IceCube. I also used Graph Neural Networks

<sup>4</sup> Copyright by

<sup>5</sup> DANIEL NICHOLAS SALAZAR-GALLEGOS

<sup>6</sup> Today

## ACKNOWLEDGMENTS

8 I love my friends. Thanks to everyone that helped me figure this out. Amazing thanks to the people  
9 at LANL who supported me. Eames, etc Dinner Parties Jenny and her child Kaydince Kirsten, Pat,  
10 Andrea Family. You're so far but so critical to my formation. Unconditional love. Roommate

**TABLE OF CONTENTS**

12

## LIST OF TABLES

13

Proof I know how to include

**LIST OF FIGURES**

**LIST OF ABBREVIATIONS**

- 16 **MSU** Michigan State University
- 17 **LANL** Los Alamos National Laboratory
- 18 **DM** Dark Matter
- 19 **SM** Standard Model
- 20 **HAWC** High Altitude Water Cherenkov Observatory

## **CHAPTER 1**

### **INTRODUCTION**

22 Is the text not rendering right? Ah ok it knows im basically drafting the doc still

## CHAPTER 2

23

### DARK MATTER IN THE COSMOS

24 **2.1 Introduction**

25     The dark matter problem can be summarized in part by the following thought experiment.

26     Let us say you are the teacher for an elementary school classroom. You take them on a field  
27 trip to your local science museum and among the exhibits is one for mass and weight. The exhibit  
28 has a gigantic scale, and you come up with a fun problem for your class.

29     You ask your class, "What is the total weight of the classroom? Give your best estimation to  
30 me in 30 minutes, and then we'll check your guess on the scale. If your guess is within 10% of the  
31 right answer, we will stop for ice cream on the way back."

32     The students are ecstatic to hear this, and they get to work. The solution is some variation of  
33 the following strategy. The students should give each other their weight or best guess if they do  
34 not know. Then, all they must do is add each student's weight and get a grand total for the class.  
35 The measurement on the giant scale should show the true weight of the class. When comparing  
36 the measured weight to your estimation, multiply the measurement by  $1.0 \pm 0.1$  to get the  $\pm 10\%$   
37 tolerances for your estimation.

38     Two of your students, Sandra and Mario, return to you with a solution.

39     They say, "We weren't sure of everyone's weight. We used 65 lbs. for the people we didn't  
40 know and added everyone who does know. There are 30 of us, and we got 2,000 lbs.! That's a ton!"

41     You estimated 1,900 lbs. assuming the average weight of a student in your class was 60 lbs.  
42 So, you are pleased with Sandra's and Mario's answer. You instruct your students to all gather on  
43 the giant scale and read off the weight together. To all your surprise, the scale reads *10,000 lbs.*!  
44 10,000 is significantly more than a 10% error from 2,000. In fact, it is approximately 5 times more  
45 massive than either your or your students' estimates. You think to yourself and conclude there  
46 must be something wrong with the scale. You ask an employee to check the scale and verify it is  
47 well calibrated. They confirm that the scale is in working order. You weigh a couple of students  
48 individually to assess that the scale is well calibrated. Sandra weighs 59 lbs., and Mario weighs

49 62 lbs., typical weights for their age. You then weigh each student individually and see that their  
50 weights individually do not deviate greatly from 60 lbs. So, where does all the extra weight come  
51 from?

52 This thought experiment serves as an analogy to the Dark Matter problem. The important  
53 substitution to make however is to replace the students with stars and the classroom with a galaxy,  
54 say the Milky Way. Individually the mass of stars is well measured and defined with the Sun as our  
55 nearest test case. However, when we set out to measure the mass of a collection of stars as large as  
56 galaxies, our well-motivated estimation is wildly incorrect. There simply is no way to account for  
57 this discrepancy except without some unseen, or dark, contribution to mass and matter in galaxies.  
58 I set out in my thesis to narrow the possibilities of what this Dark Matter could be.

59 This chapter is organized like the following... **TODO: Text should look like ... Chapter x has**  
60 **blah blah blah.**

## 61 2.2 Dark Matter Basics

62 Presently, a more compelling theory of cosmology that includes Dark Matter (DM) in order  
63 to explain a variety of observations is  $\Lambda$  Cold Dark Matter, or  $\Lambda$ CDM. I present the evidence  
64 supporting  $\Lambda$ CDM in ?? yet discuss the conclusions of the  $\Lambda$ CDM model here. According to  
65  $\Lambda$ CDM fit to observations on the Cosmic Microwave Background (CMB), DM is 26.8% of the  
66 universe's current energy budget. Baryonic matter, stuff like atoms, gas, and stars, contributes to  
67 4.9% of the universe's current energy budget [1, 2, 3].

68 DM is dark; it does not interact readily with light at any wavelength. DM also does not interact  
69 noticeably with the other standard model forces (Strong and Weak) at a rate that is readily observed  
70 [3]. DM is cold, which is to say that the average velocity of DM is below relativistic speeds [1].  
71 'Hot' DM would not likely manifest the dense structures we observe like galaxies, and instead  
72 would produce much more diffuse galaxies than what is observed [3, 1]. DM is old; it played a  
73 critical role in the formation of the universe and the structures within it [1, 2].

74 Observations of DM have so far been only gravitational. The parameter space available to what  
75 DM could be therefore is extremely broad. The broad DM parameter space is iteratively tested in

76 DM searches by supposing a hypothesis that has not yet been ruled out and performing observations  
77 to test them. When the observations yield a null result, the parameter space is constrained further.  
78 I present some approaches for DM searches in ??.

79 **2.3 Evidence for Dark Matter**

80 Dark Matter (DM) has been a looming problem in physics for almost 100 years. Anomalies  
81 have been observed by astrophysicists in galactic dynamics as early as 1933 when Fritz Zwicky  
82 noticed unusually large velocity dispersion in the Coma cluster. Zwicky's measurement was the  
83 first recorded to use the Virial theorem to measure the mass fraction of visible and invisible matter  
84 in celestial bodies [4]. From Zwicky in [5], "*If this would be confirmed, we would get the surprising*  
85 *result that dark matter is present in much greater amount than luminous matter.*" Zwicky's and  
86 others' observation did not instigate a crisis in astrophysics because the measurements did not  
87 entirely conflict with their understanding of galaxies [4]. In 1978, Rubin, Ford, and Norbert  
88 measured rotation curves for ten spiral galaxies [6]. Rubin et al.'s 1978 publication presented a  
89 major challenge to the conventional understanding of galaxies that could no longer be dismissed by  
90 measurement uncertainties. Evidence has been mounting ever since for this exotic form of matter.  
91 The following subsections provide three compelling pieces of evidence in support of the existence  
92 of DM.

93 **2.3.1 First Clues: Stellar Velocities**

94 Zwicky, and later Rubin, measured the stellar velocities of various galaxies to estimate their  
95 virial mass. The Virial Theorem upon which these observations are interpreted is written as

$$2T + V = 0. \quad (2.1)$$

96 Where  $T$  is the kinetic energy and  $V$  is the potential energy in a self-gravitating system. The  
97 classical Newton's law of gravity from stars and gas was used for gravitational potential modeled in  
98 the observed galaxies:

$$V = -\frac{1}{2} \sum_i \sum_{j \neq i} \frac{m_i m_j}{r_{ij}}. \quad (2.2)$$

99 Zwicky et al. measured just the velocities of stars apparent in optical wavelengths [5]. Rubin et al.  
 100 added by measuring the velocity of the hydrogen gas via the 21 cm emission line of Hydrogen [6].  
 101 The velocities of the stars and gas are used to infer the total mass of galaxies and galaxy clusters via  
 102 ???. An inferred mass is obtained from the luminosity of the selected sources. The two inferences  
 103 are compared to each other as a luminosity to mass ratio which typically yielded [1]

$$\frac{M}{L} \sim 400 \frac{M_{\odot}}{L_{\odot}} \quad (2.3)$$

104  $M_{\odot}$  and  $L_{\odot}$  referring to stellar mass and stellar luminosity, respectively. These ratios clearly indicate  
 105 a discrepancy in apparent light and mass from stars and gas and their velocities.

106 Rubin et al. [6] demonstrated that the discrepancy was unlikely to be an underestimation of  
 107 the mass of the stars and gas. The inferred "dark" mass was up to 5 times more than the luminous  
 108 mass. This dark mass also needed to extend well beyond the extent of the luminous matter.

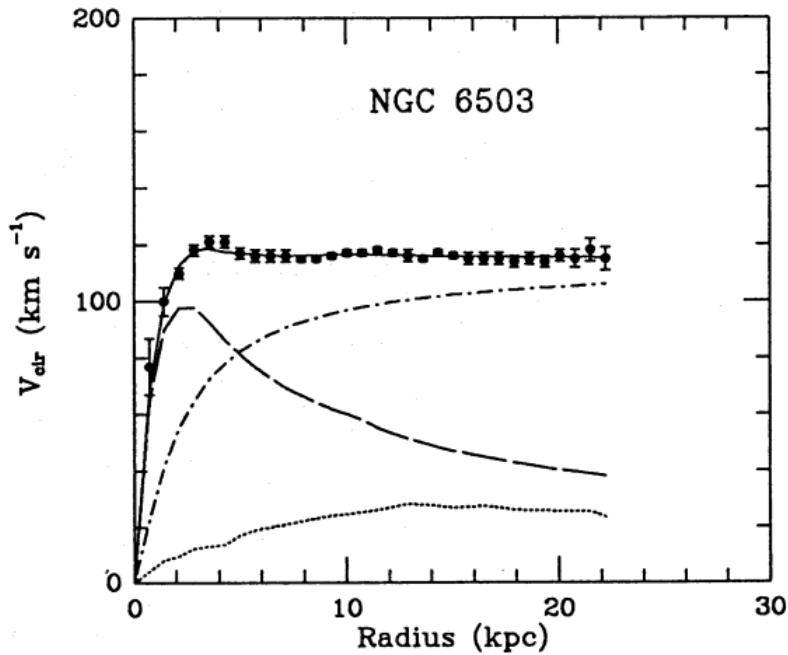


Figure 2.1 Rotation curve fit to NGC 6503 from [7]. Dashed line is the contribution from visible matter. Dotted curves are from gas. Dash-dot curves are from dark matter (DM). Solid line is the composite contribution from all matter and DM sources. Data are indicated with bold dots with error bars. Data agree strongly with a matter + DM composite prediction.

109 ?? features one of many rotation curves plotted from the stellar velocities within galaxies. The

110 measured rotation curves mostly feature a flattening of velocities at higher radius which is not  
111 expected if the gravity was only coming from gas and luminous matter. The extension of the  
112 flat velocity region also indicates that the DM is distributed far from the center of the galaxy.  
113 Modern velocity measurements include significantly larger objects, galactic clusters, and smaller  
114 objects, dwarf galaxies. Yet, measurements along this regime are leveraging the Virial theorem  
115 with Newtonian potential energies. We know Newtonian gravity is not a comprehensive description  
116 of gravity. New observational techniques have been developed since 1978, and those are discussed  
117 in the following sections.

118 **2.3.2 Evidence for Dark Matter: Gravitational Lensing**

119 Modern evidence for dark matter comes from new avenues beyond stellar velocities. Grav-  
120 itational lensing from DM is a new channel from general relativity. General relativity predicts  
121 aberrations in light caused by massive objects. In recent decades we have been able to measure  
122 the lensing effects from compact objects and DM halos. ?? shows how different massive objects  
123 change the final image of a faraway galaxy resulting from gravitational lensing. Gravitational  
124 lensing developed our understanding of dark matter in two important ways.

125 Gravitational lensing provides additional compelling evidence for DM. The observation of two  
126 merging galactic clusters in 2006, shown in ??, provided a compelling argument for DM outside  
127 the Standard Model. These clusters merged recently in astrophysical time scales. Galaxies and  
128 star cluster have mostly passed by each other as the likelihood of their collision is low. Therefore,  
129 these massive objects will mostly track the highest mass, dark and/or baryonic, density. Yet, the  
130 intergalactic gas is responsible for the majority of the baryonic mass in the systems [4]. These gas  
131 bodies will not phase through and will heat up as they collide together. The hot gas is located via  
132 x-ray emission from the cluster. Two observations of the clusters were performed independently of  
133 each other.

134 The first was the lensing of light around the galaxies due to their gravitational influences. When  
135 celestial bodies are large enough, the gravity they exert bends space and time itself. The warped  
136 space-time lenses light and will deflect in an analogous way to how glass lenses will bend light, see

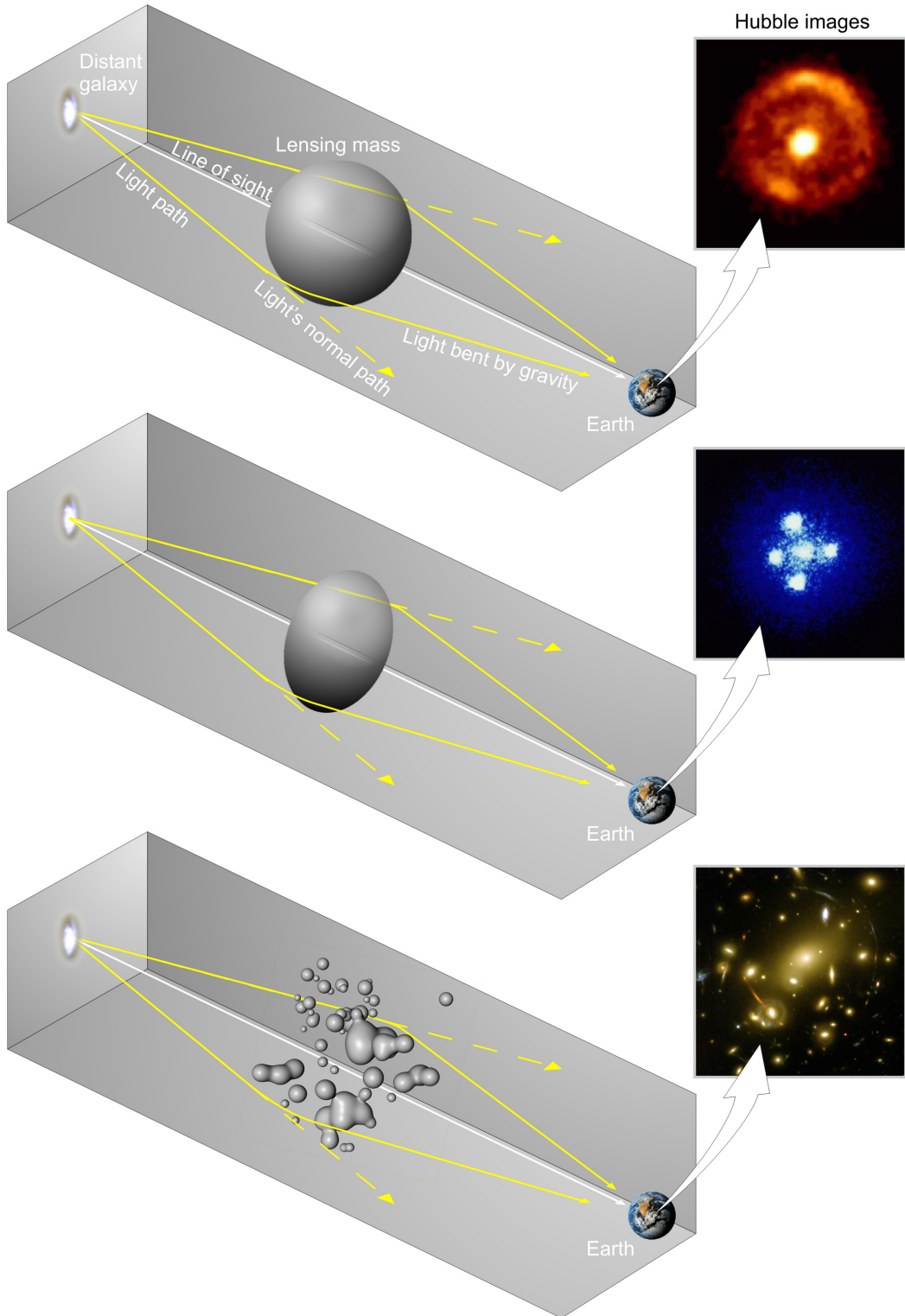


Figure 2.2 Light from distant galaxy is bent in unique ways depending on the distribution of mass between the galaxy and Earth. Yellow dashed lines indicate where the light would have gone if the matter were not present [8].

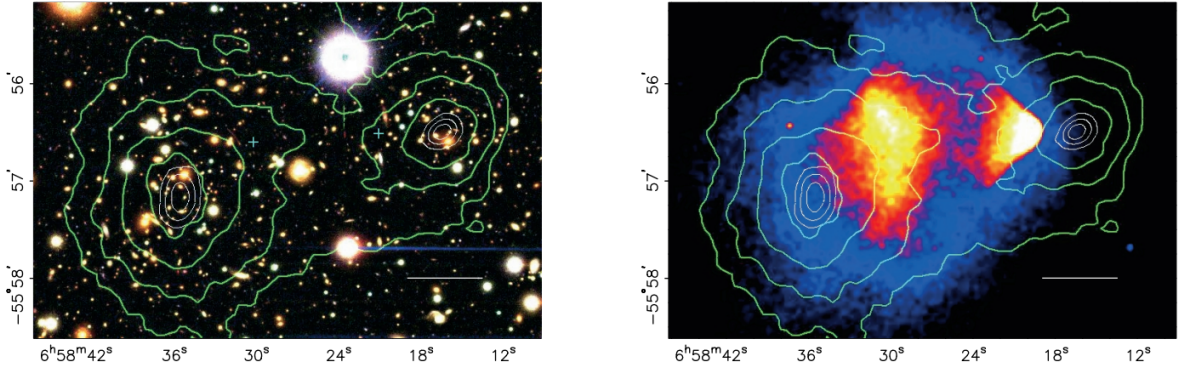


Figure 2.3 (left) Optical image of galactic cluster 1E0657-558. (right) X-ray image of the cluster with redder meaning hotter and higher baryon density. (both) Green contours are reconstruction of gravity contours from weak lensing. White rings are the best fit mass maxima at 68.3%, 95.5%, and 99.7% confidence. The matter maxima of the clusters are clearly separated from x-ray maxima. [9]

137 ???. With a sufficient understanding of light sources behind a massive object, we can reconstruct  
 138 the contours of the gravitational lenses. The gradient of the contours shown in ?? then indicates  
 139 how dense the matter is and where it is.

140 The x-ray emission can then be observed from the clusters. Since these galaxies are mostly gas  
 141 and are merging, then the gas should be getting hotter. If they are merging, the x-ray emissions  
 142 should be the strongest where the gas is mostly moving through each other. Hence, X-ray emission  
 143 maps out where the gas is in the merging galaxy cluster.

144 The lensing and x-ray observations were done on the Bullet cluster featured on ???. The x-ray  
 145 emissions do not align with the gravitational contours from lensing. The incongruence in mass  
 146 density and baryon density suggests that there is a lot of matter somewhere that does not interact  
 147 with light. Moreover, this dark matter cannot be baryonic [9]. The Bullet Cluster measurement did  
 148 not really tell us what DM is exactly, but it did give the clue that DM also does not interact with  
 149 itself very strongly. If DM did interact strongly with itself, then it would have been more aligned  
 150 with the x-ray emission [9]. There have been follow-up studies of galaxy clusters with similar  
 151 results. The Bullet Cluster and others like it provide a persuasive case against something possibly  
 152 amiss in our gravitational theories.

153 **2.3.3 Evidence for Dark Matter: Cosmic Microwave Background**

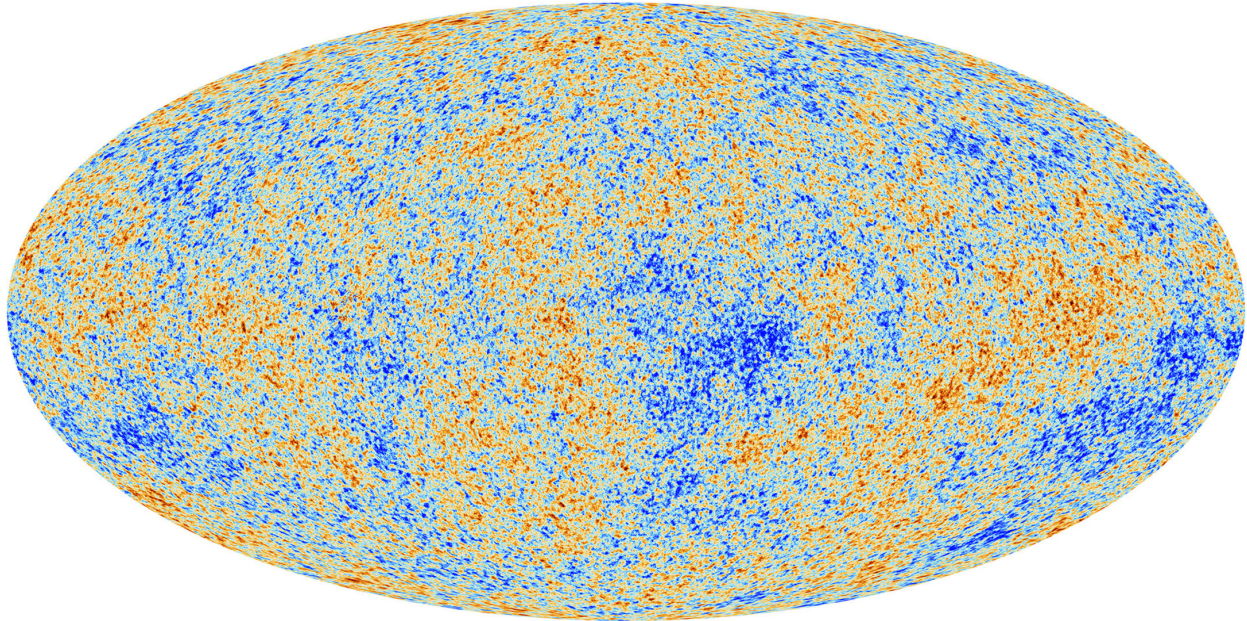


Figure 2.4 Plank CMB sky. Sky map features small variations in temperature in primordial light. These anisotropies are used to make inferences about the universe's energy budget and developmental history. [10]

154     The Cosmic Microwave Background (CMB) is the primordial light from the early universe  
155    when Hydrogen atoms formed from the free electron and proton soup in the early universe. The  
156    CMB is the earliest light we can observe; released when the universe was about 380,000 years old.  
157    Then we look at how the simulated universes look like compared to what we see. ?? is the most  
158    recent CMB image from the Plank satellite after subtracting the average value and masking the  
159    galactic plane [10]. Redder regions indicate a slightly hotter region in the CMB, and blue indicates  
160    colder. The intensity variations are on the order of 1 in 1000 with respect to the average value.

161     The Cosmic Microwave Background shows that the universe had DM in it from an incredibly  
162    early stage. To measure the DM, Dark Energy, and matter fractions of the universe from the CMB,  
163    the image is analyzed into a power spectrum, which shows the amplitude of the fluctuations as  
164    a function of spherical multipole moments.  $\Lambda$ CDM provides the best fit to the power spectra of  
165    the CMB as shown in ?. The CMB power spectrum is quite sensitive to the fraction of each  
166    energy contribution in the early universe. Low  $l$  modes are dominated by variations in gravitational

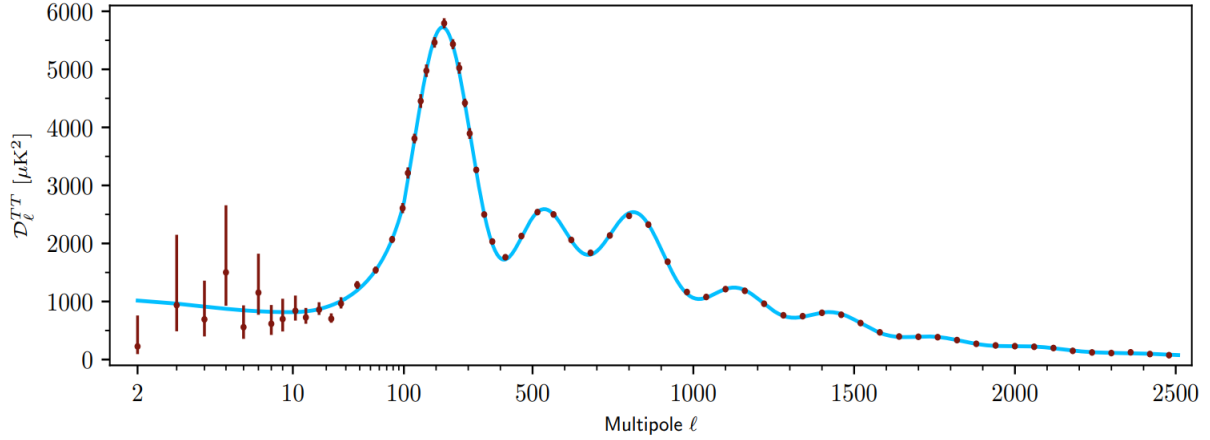


Figure 2.5 Observed Cosmic Microwave Background power spectrum as a function of multipole moment from Plank [10]. Blue line is best fit model from  $\Lambda$ CDM. Red points and lines are data and error, respectively.

167 potential. Intermediate  $l$  emerge from oscillations in photon-baryon fluid from competing baryon  
 168 pressures and gravity. High  $l$  is a damped region from the diffusion of photons during electron-  
 169 proton recombination. [1]

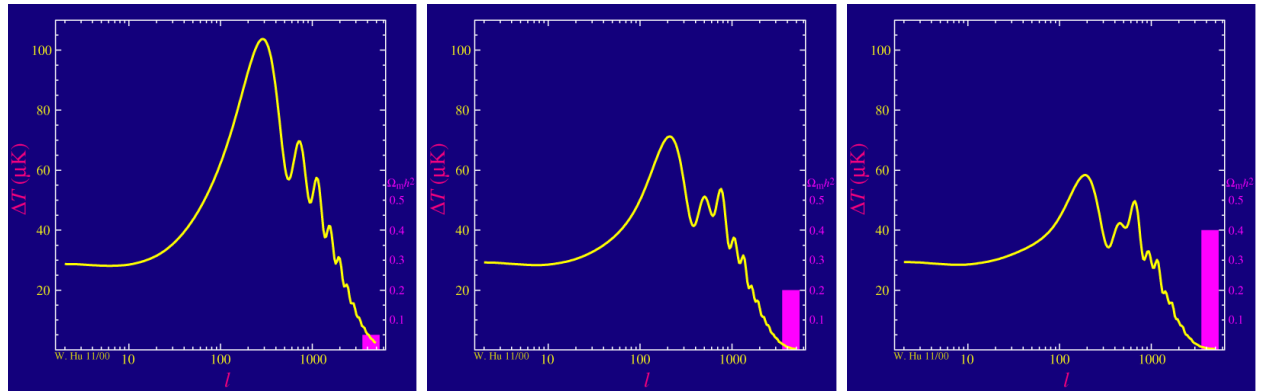


Figure 2.6 Predicted power spectra of CMB for different  $\Omega_m h^2$  values for fixed baryon density from [11]. (left) Low  $\Omega_m h^2$  increases the prominence of first and second peaks. (middle)  $\Omega_m h^2$  is most similar to the observed power spectrum. The second and third peaks are similar in height. (right)  $\Omega_m h^2$  is large which suppresses the first peak and raises the prominence of the third peak.

170 The harmonics would look quite different for a universe with less DM. ?? demonstrates the  
 171 effect  $\Omega_m h^2$  has on the expected power spectrum for fixed baryon matter density. [11] Sweeping  
 172  $\Omega_m h^2$  in this way clearly shows the effect dark matter has on the CMB power spectrum. The  
 173 observations fit well with the  $\Lambda$ CDM model, and the derived fractions are as follows. The matter

174 fraction:  $\Omega_m = 0.3153$ ; and the baryon fraction:  $\Omega_b = 0.04936$  [10]. Plank's observations also  
175 provide a measure of the Hubble constant,  $H_0$ .  $H_0$  especially has seen a growing tension in the  
176 past decade that continues to deepened with observations from instruments like the James Webb  
177 Telescope [12, 13]. As Hubble tensions deepen, we may find that perhaps  $\Lambda$ **CDM**, despite its  
178 successes, is missing some critical physics.

179 Overall, the Newtonian motion of stars in galaxies, weak lensing from galactic clusters, and  
180 power spectra from primordial light form a compelling body of research in favor of dark matter.  
181 It takes another leap of theory and experimentation to make observations of DM that are non-  
182 gravitational in nature. In ??, the evidence for DM implies strongly that the DM is matter and  
183 not a lost parameter in the gravitational fields between massive objects. Finally, if we take one  
184 axiom: that this matter has quantum behavior, such as being described by some Bohr wavelength  
185 and abiding by some fermion or boson statistics; then we arrive at particle dark matter. One particle  
186 DM hypothesis is the Weakly Interacting Massive Particle (WIMP). This DM candidate theory is  
187 discussed further in the next section and is the focus of this thesis.

## 188 2.4 Searching for Dark Matter: Particle DM

189 ?? shows the Standard Model of particle physics and is currently the most accurate model for  
190 the dynamics of fundamental particles like electrons and photons. The current status of the SM  
191 does not have a viable DM candidate. When looking at the standard model, we can immediately  
192 exclude any charged particle because charged particles interact strongly with light. Specifically,  
193 this will rule out the following charged, fundamental particles:  $e, \mu, \tau, W, u, d, s, c, t, b$  and their  
194 corresponding antiparticles. Recalling from ?? that DM must be long-lived and stable over the  
195 age of the universe which excludes all SM particles with decay half-lives at or shorter than the age  
196 of the universe. The lifetime constraint additionally eliminates the  $Z$  and  $H$  bosons. Finally, the  
197 candidate DM needs to be somewhat massive. Recall from ?? that DM is cold or not relativistic  
198 through the universe. This eliminates the remaining SM particles:  $\nu_{e,\mu,\tau}, g, \gamma$  as DM candidates.  
199 Because there are no DM candidates within the SM, the DM problem strongly hints to physics  
200 beyond the SM (BSM).

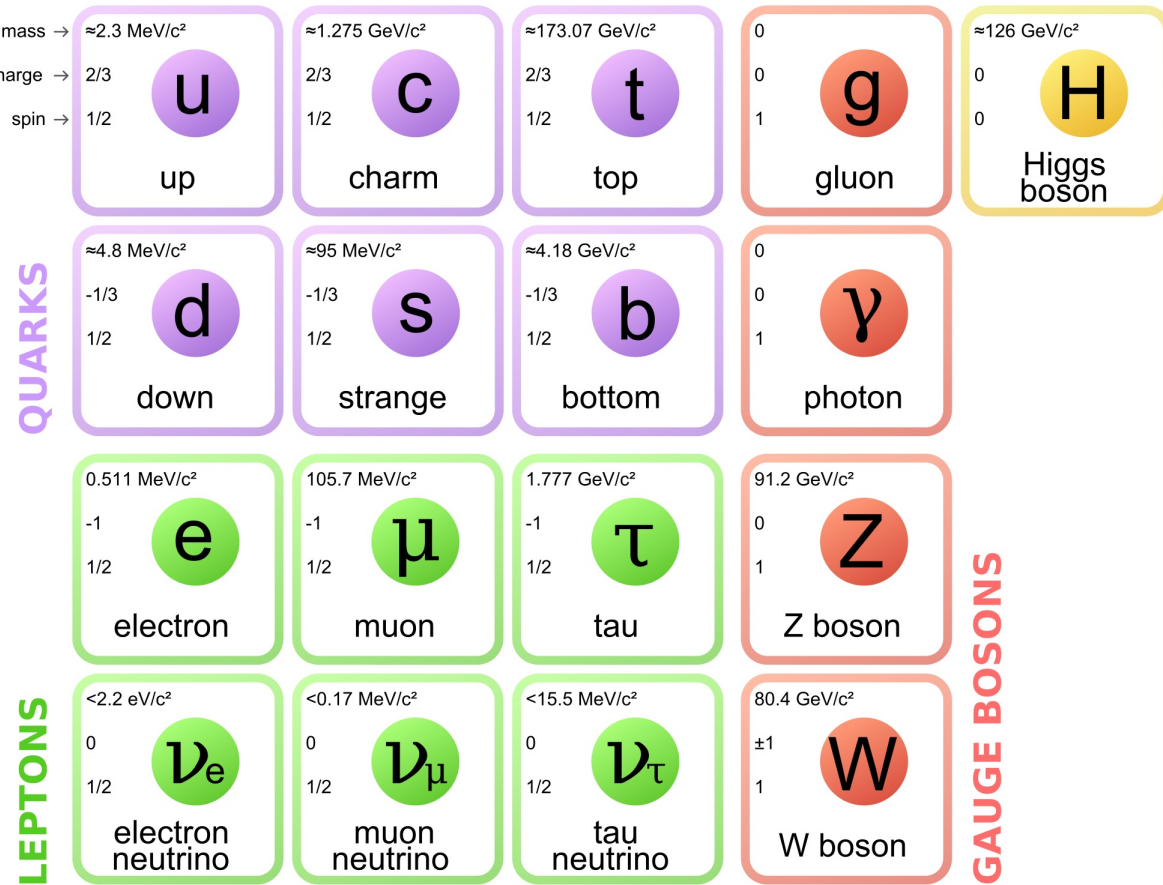


Figure 2.7 The Standard Model (SM) of particle physics. Figure taken from <http://www.quantumdiaries.org/2014/03/14/the-standard-model-a-beautiful-but-flawed-theory/>

### 201 2.4.1 Shake it, Break it, Make it

202 When considering DM that couples in some way with the SM, the interactions are roughly  
 203 demonstrated by interaction demonstrated in ???. The figure is a simplified Feynman diagram  
 204 where the arrow of time represents the interaction modes of: **Shake it, Break it, Make it.**

205 **Shake it** refers to the direct detection of dark matter. Direct detection interactions start with  
 206 a free DM particle and an SM particle. The DM and SM interact via elastic or inelastic collision  
 207 and recoil away from each other. The DM remains in the dark sector and imparts some momentum  
 208 onto the SM particle. The hope is that the momentum imparted onto the SM particle is sufficiently  
 209 high enough to pick up with extremely sensitive instruments. Because we cannot create the DM in  
 210 the lab, a direct detection experiment must wait until DM is incident on the detector. Most direct  
 211 detection experiments are therefore placed in low-background environments with inert detection

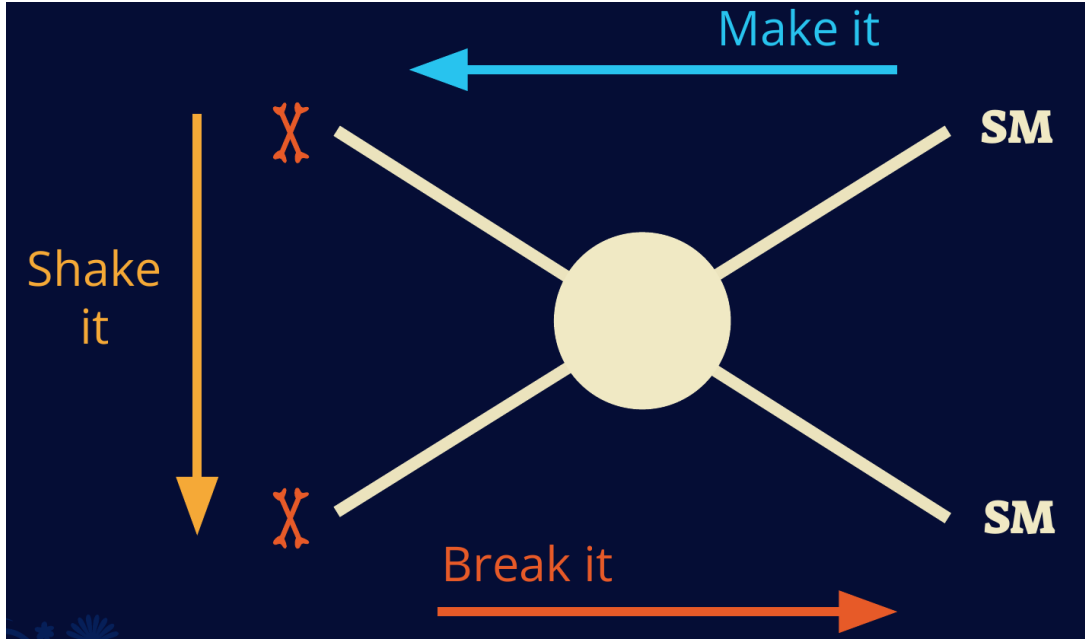


Figure 2.8 Simplified Feynman diagram demonstrating different ways DM can interact with SM particles. The 'X's refer to the DM particles whereas the SM refer to fundamental particles in the SM. The large circle in the center indicates the vertex of interaction and is purposely left vague. The colored arrows refer to different directions of time as well as their respective labels. The arrows indicate the initial and final state of the DM -SM interaction in time.

<sup>212</sup> media like the noble gas Xenon. [14]

<sup>213</sup> **Make it** refers to the production of DM from SM initial states. The experiment starts with  
<sup>214</sup> particles in the SM. These SM particles are accelerated to incredibly high energies and then  
<sup>215</sup> collide with each other. In the confluence of energy, DM hopefully emerges as a byproduct of the  
<sup>216</sup> SM annihilation. Often it is the collider experiments that are energetic enough to hypothetically  
<sup>217</sup> produce DM. These experiments include the world-wide collaborations ATLAS and CMS at CERN  
<sup>218</sup> where proton collide together at extreme energies. The DM searches, however, are complex. DM  
<sup>219</sup> likely does not interact with the detectors and lives long enough to escape the detection apparatus of  
<sup>220</sup> CERN's colliders. This means any DM production experiment searches for an excess of events with  
<sup>221</sup> missing momentum or energy in the events. An example event with missing transverse momentum  
<sup>222</sup> is shown in ???. The missing momentum with no particle tracks implies a neutral particle carried  
<sup>223</sup> the energy out of the detector. However, there are other neutral particles in the SM, like neutrons  
<sup>224</sup> or neutrinos, so any analysis has to account for SM signatures of missing momentum. [15]

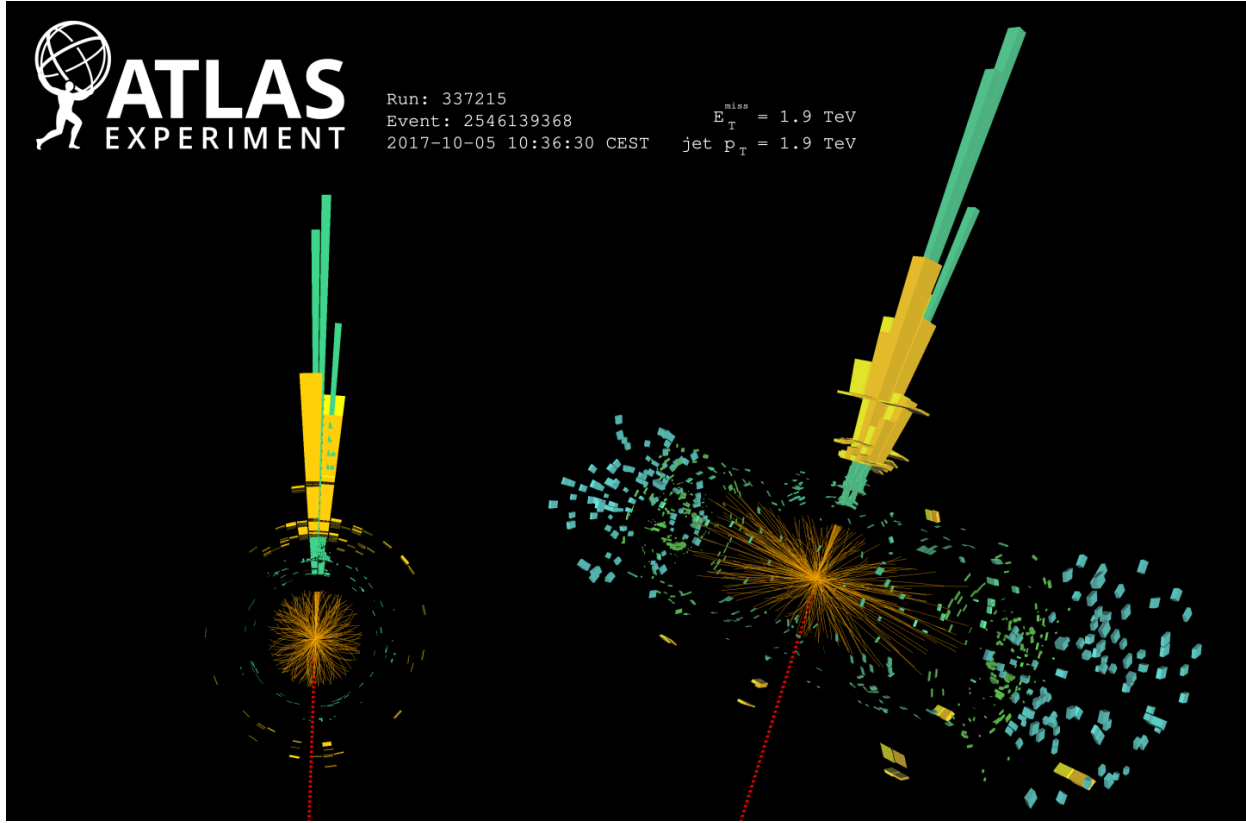


Figure 2.9 A single jet event in ATLAS detector from 2017 [16]. Jet momentum was observed to be 1.9 TeV. Missing transverse momentum was observed to be 1.9 TeV compared to the initial transverse momentum of the event was 0. Implied MET is traced by a red dashed line in event display.

#### 225 2.4.2 Break it: Standard Model Signatures of Dark Matter through Indirect Searches

226 **Break it** refers to the creation of SM particles from the dark sector, and it is the primary focus  
 227 of this thesis. The interaction begins with DM or in the dark sector. The hypothesis is that this  
 228 DM will either annihilate with itself or decay and produce an SM byproduct. This method is  
 229 often referred to as the Indirect Detection of DM because we have no lab to directly control or  
 230 manipulate the DM. Therefore, most indirect DM searches are performed using observations of  
 231 known DM densities among the astrophysical sources. The strength is that we have the whole of the  
 232 universe and its 13.6-billion-year lifespan to use as a detector and particle accelerator. Additionally,  
 233 locations of dark matter are well cataloged since it was astrophysical observations that presented  
 234 the problem of DM in the first place.

235 However, anything can happen in the universe. There are many difficult to deconvolve back-

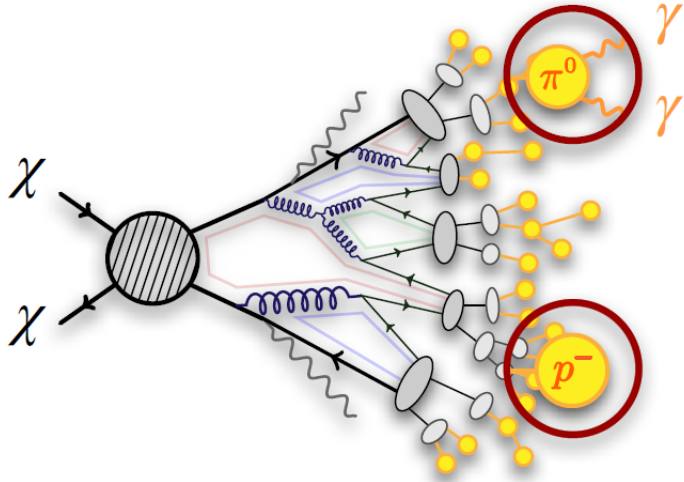


Figure 2.10 More detailed pseudo-Feynman diagram of particle cascade from dark matter annihilation into 2 quarks. The quarks hadronize and down to stable particles like  $\gamma$  or the anti-proton ( $p^-$ ). Diagram pulled from ICRC 2021 presentation on DM annihilation search [17].

236 grounds when searching for DM. One prominent example is the galactic center. We know the  
 237 galactic center has a large DM content because of stellar kinematics in our Milky Way and DM halo  
 238 simulations. Yet, any signal from the galactic center is challenging to parse apart from the extreme  
 239 environment of our supermassive black hole, unresolved sources, and diffuse emission from the  
 240 interstellar medium [18]. Despite the challenges, any DM model that yields evidence in the other  
 241 two observation methods, **Shake it or Make it** must be corroborated with indirect observations of  
 242 the known DM sources. Without corroborating evidence, DM observation in the lab is hard-pressed  
 243 to demonstrate that it is the model contributing to the DM seen at the universal scale.

244 In the case of WIMP DM, signals are described in terms of primary SM particles produced  
 245 from DM decay or annihilation. The SM initial state particles are then simulated down to stable  
 246 final states such as the  $\gamma$ ,  $\nu$ ,  $p$ , or  $e$  which can traverse galactic lengths to reach Earth.

247 ?? shows the quagmire of SM particles that emerges from SM initial states that are not stable  
 248 [17]. There are many SM particles with varying energies that can be produced in such an interaction.  
 249 For any arbitrary DM source and stable SM particle, the SM flux from DM annihilating to a neutral

250 particle in the SM,  $\phi$ , from a region in the sky is described by the following.

$$\frac{d\Phi_\phi}{dE_\phi} = \frac{\langle\sigma v\rangle}{8\pi m_\chi^2} \frac{dN_\phi}{dE_\phi} \times \int_{\text{source}} d\Omega \int_{l.o.s} \rho_\chi^2 dl(r, \theta') \quad (2.4)$$

251 In ??,  $\langle\sigma v\rangle$  is the velocity-weighted annihilation cross-section of DM to the SM.  $m_\chi$  refers to the  
252 mass of DM, noted with Greek letter  $\chi$ .  $\frac{dN_\phi}{dE_\phi}$  is the N particle flux weighted by the particle energy.  
253 An example is provided in ?? for the  $\gamma$  final state. The integrated terms are performed over the  
254 solid angle,  $d\Omega$ , and line of sight, l.o.s.  $\rho$  is the density of DM for a location  $(r, \theta')$  in the sky. The  
255 terms left of the 'x' are often referred to as the particle physics component. The terms on the right  
256 are referred to as the astrophysical component. For decaying DM, the equation changes to...

$$\frac{d\Phi_\phi}{dE_\phi} = \frac{1}{4\pi\tau m_\chi} \frac{dN_\phi}{dE_\phi} \times \int_{\text{source}} d\Omega \int_{l.o.s} \rho_\chi dl(r, \theta') \quad (2.5)$$

257 In ??,  $\tau$  is the decay lifetime of the DM. Just as in ??, the left and right terms are the particle physics  
258 and the astrophysical components respectively. The integrated astrophysical component of ?? is  
259 often called the J-Factor. Whereas the integrated astrophysical component of ?? is often called the  
260 D-Factor.

261 Exact DM  $\text{DM} \rightarrow \text{SM}$  branching ratios are not known, so it is usually assumed to go 100%  
262 into an SM particle/anti-particle. Additionally, when a DM annihilation or decay produces one of  
263 the neutral, long-lived SM particles ( $\nu$  or  $\gamma$ ), the particle is traced back to a DM source. For DM  
264 above GeV energies, there are very few SM processes that can produce particles with such a high  
265 energy. Seeing such a signal would almost certainly be an indication of the presence of dark matter.  
266 Fortunately, the universe provides us with the largest volume and lifetime ever for a particle physics  
267 experiment.

## 268 **2.5 Sources for Indirect Dark Matter Searches**

269 The first detection of DM relied on optical observations. Since then, we have developed new  
270 techniques to find DM dense regions. As described in ??, many DM dense regions were through  
271 observing galactic rotation curves. Our Milky Way galaxy is among DM dense regions discovered,  
272 and it is the largest nearby DM dense region to look at. Additionally, the DM halo surrounding the  
273 Milky Way is clumpy [18]. There are regions in the DM halo of the Milky Way that have more DM

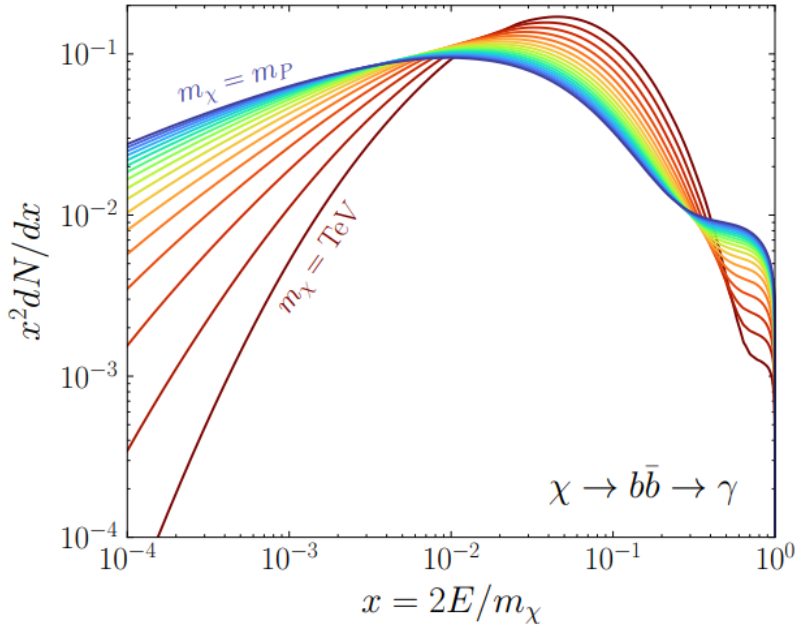


Figure 2.11 Dark Matter (DM) decay spectrum for  $b\bar{b}$  initial state and  $\gamma$  final state. Redder spectra are for larger DM masses. Bluer spectra are light DM masses.  $x$  is a unitless factor defined as the ratio of the mass of DM,  $m_\chi$ , and the final state particle energy  $E_\gamma$ . Figure from [19].

than others that have captured gas over time. These sub-halos were dense enough collapse gas and form stars. These apparent sub galaxies are known as dwarf spheroidal galaxies and are the main sources studied in this thesis. Each source type comes with different trade-offs. Galactic Center studies will be very sensitive to the assumed distribution of DM. The central DM density can vary substantially as demonstrated in ???. At distances close to the center of the galaxy, or small  $r$ , the differences in DM densities can be 3-4 orders of magnitude. Searches toward the galactic center will therefore be quite sensitive to the assumed DM distribution.

Searches toward Dwarf Spheroidal Galaxies (dSph's) suffer from uncertainties in the DM density less than the galactic center studies. This is mostly from their diminutive size being smaller than the angular resolution of most  $\gamma$ -ray observatories [18]. The DM content dSph's are typically determined with the Virial theorem, ???, and are usually majority DM [18] in mass. DSph's tend to be ideal sources to look at for DM searches. Their environments are quiet with little astrophysical background. Unlike the galactic center, the most active components of dSph's are the stars within

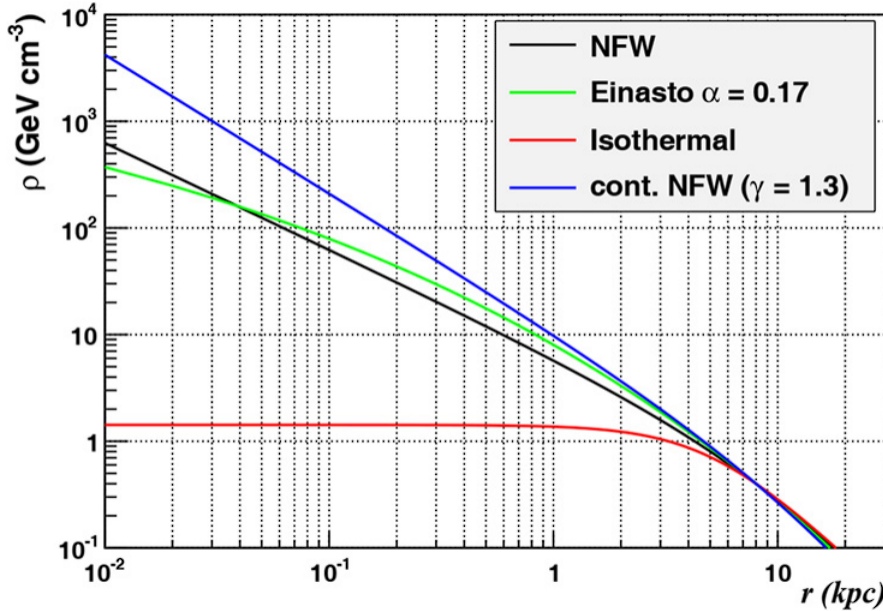


Figure 2.12 Different dark matter density profiles compared. Some models produce exceptionally large densities at small  $r$  [20].

them versus a violent accretion disc around a black hole. All this together means that dSph's are among the best sources to look at for indirect DM searches. dSph's are the targets of focus for this thesis.

## 2.6 Multi-Messenger Dark Matter

Astrophysics entered a new phase in the past few decades that leverages our increasing sensitivity to SM channels and general relativity (GR). Up until the 21st century, astrophysical observations were performed with photons ( $\gamma$ ) only. Astrophysics with this 'messenger' is fairly mature now. Novel observations of the universe have since only adjusted the sensitivity of the wavelength of light that is observed except at MeV energies. Gems like the CMB [10], and more have ultimately been observations of different wavelengths of light. Multi-messenger astrophysics proposes using other SM particles such as the  $p^{+/-}$ , or  $\nu$  or gravitation waves predicted by general relativity.

The experiment LIGO had a revolutionary discovery in 2016 with the first detection of a binary black hole merger [21]. This opened the collective imagination to observing the universe through gravitational waves. There has also been a surge of interest in the neutrino ( $\nu$ ) sector. IceCube

301 demonstrated that we are sensitive to neutrinos in regions that correlate with significant photon  
 302 emission like the galactic plane [22]. Neutrinos, like gravitational waves and light, travel mostly  
 303 unimpeded from their source to our observatories. This makes pointing to the originating source  
 304 of these messengers much easier than it is for cosmic rays which are deflected from their source by  
 305 magnetic fields.

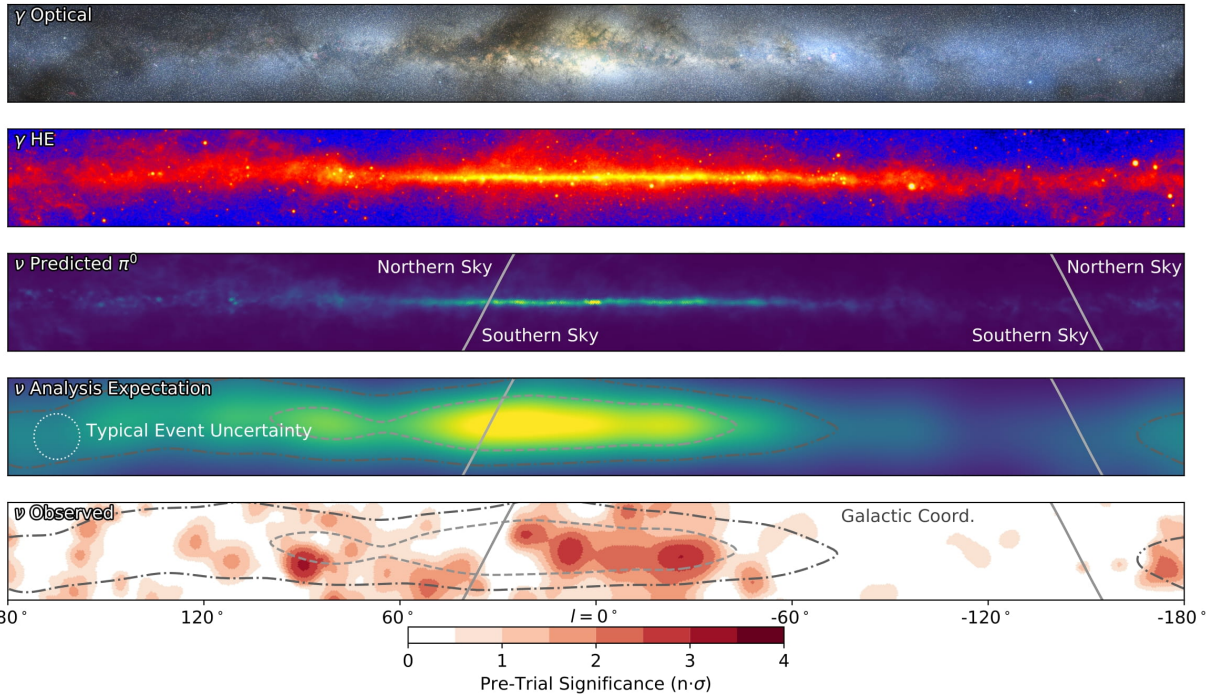


Figure 2.13 The Milky Way Galaxy in photons ( $\gamma$ ) and neutrinos ( $\nu$ ) [22]. The Galactic center is at  $l=0^\circ$  and is the brightest region in all panels. (top) An Optical color image of the Milky Way galaxy seen from Earth. Clouds of gas and dust obscure some light from stars. (2nd down) Integrated flux of  $\gamma$ -rays observed by the Fermi-LAT telescope [23]. (middle) Expected neutrino emission that corresponds with Fermi-LAT observations. (2nd up) Expected neutrino emission profile after considering detector systematics of IceCube. (bottom) Observed neutrino emission from region of the galactic plane. Substantial neutrino emission was detected.

306 The IceCube collaboration recently published a groundbreaking result of the Milky Way in  
 307 neutrinos. The recent result from IceCube, shown in ??, proves that we can make observations  
 308 under different messenger regimes. The top two panels show the appearance of the galactic plane  
 309 to different wavelengths of light. Some sources are more apparent in some panels, while others are  
 310 not. This new channel is powerful because neutrinos are readily able to penetrate through gas and

311 dust in the Milky Way. This new image also refines our understanding of how high energy particles  
 312 are produced. For example, the fit to IceCube data prefers neutrino production from the decay of  
 313  $\pi^0$  [22].

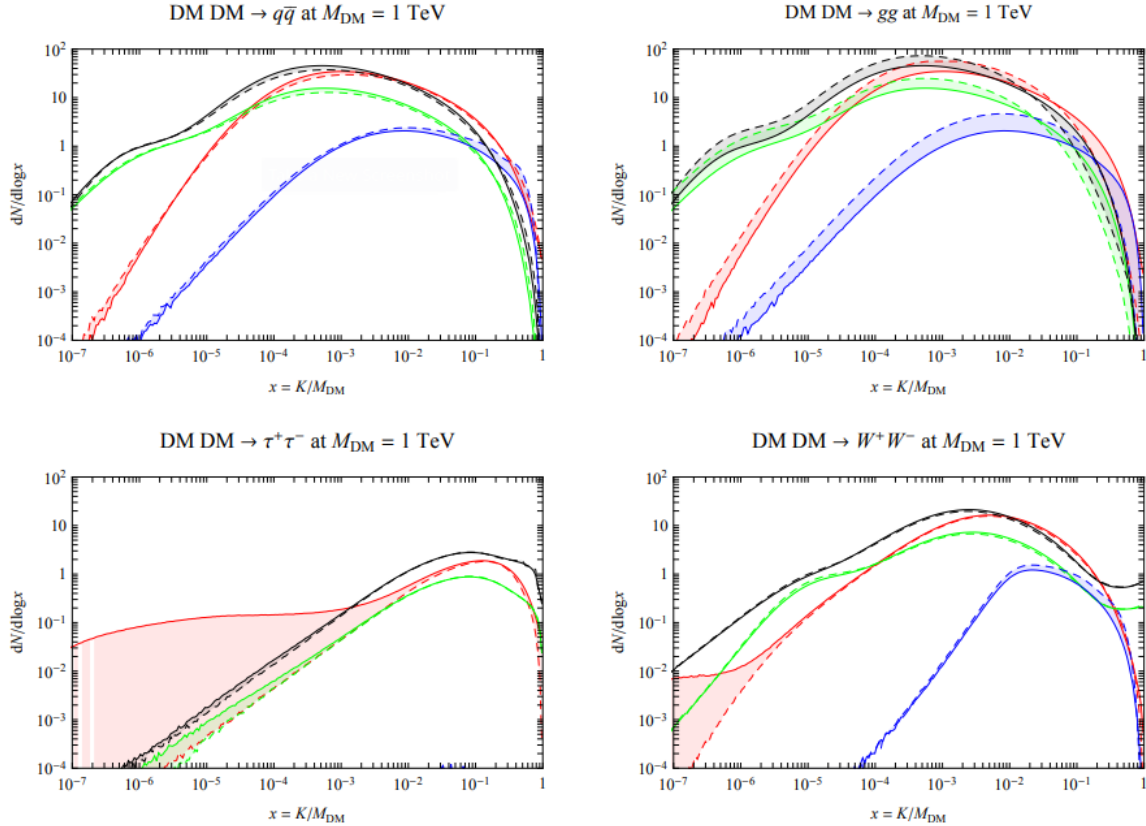


Figure 2.14 Dark Matter annihilation spectra for different final state particle and standard model annihilation channels [24]. Photons (red),  $e^\pm$  (green),  $\bar{p}$  (blue),  $\nu$  (black).

314 Exposing our observations to more cosmic messengers greatly increases our sensitivity to rare  
 315 processes. In the case of DM, ??, there are many SM particles produced in DM annihilation.  
 316 Among the final state fluxes are gammas and neutrinos. Charged particles are also produced  
 317 however they would not likely make it to Earth since they will be deflected by magnetic fields  
 318 between the source and Earth. This means observatories that can see the neutral messengers are  
 319 especially good for DM searches and for combining data for a multi-messenger DM search.

## CHAPTER 3

### 320 MULTIMESSENGER ASTROPHYSICS: DETECTING HIGH ENERGY NEUTRAL 321 MESSENGERS

#### 322 3.1 Introduction

323 Before the 20th century, all astrophysics observations were optical in nature. We literally only  
324 saw things with highly magnified optical observations. Then we discovered cosmic rays. cosmic  
325 rays are charged particles, typically naked protons or H+. This was seen by Victor Hess in 19??.  
326 Around the same time we discovered neutrinos from beta decay. Sometime around 1950 we started  
327 to build neutrino detectors which were mostly sensitive to neutrinos from the sun. Finally, it was  
328 theorized that compact objects like black holes and neutron stars would create waves in space-time  
329 when they experience mergers or collisions.

330 In the 21st century, we have developed new observation techniques and detectors that are no only  
331 sensitive to these four messengers - photons ([TODO: photon](#)), neutrinos ([TODO: nu](#)), Cosmic  
332 Rays (CR), and Gravitational Wave (WV) - we're collect high energy versions of these events.  
333 For the standad model particles, we're now sensitive to all messengers above the MeV eneryg  
334 range. Additionally, the GW's were sensitive to are in the stellar mass black hole region and above  
335 within our galactic neighborhood. This means were becoming sensitive to the fundamental physics  
336 occuring within the universe and we can rely on the universe as a TeV+ particle accelerator. We  
337 also have the abaility to correlate high energy events across messengers and gain new insights on  
338 the processes that occur in our universe.

339 This thesis focuses on very high energy (VHE) gamma rays and neutrinos. These can both be  
340 observed through the water cherenkov detection technique altho not exclusively. Methods on how  
341 to detect and observe these neutral messengers are discussed ?? and ??

#### 342 3.2 Charged Particles in a Medium

343 For high enery gamma-rays and neutrinos, we can exploit the same effect that charged particles  
344 have with water. This effect is known as Cherenkov radiation. Cherenkov Radiation occurs when a  
345 charged particle, usually electrons ( $e$ ) or muons ( $\mu$ ), traverse a medium, like water, faster than the

346 speed of light in that medium. This is similar to sonic boom where an object moves through air  
347 faster than the speed of sound in air. Cherenkov radiation can therefore be thought of as an 'optic  
348 boom'. Many astro-particle physics experiments will use water as the medium as because water  
349 has a unique set of properties ideal for charged particle tracking.



Figure 3.1 TODO: Show a nuclear reactor with cherenkov radiation[NEEDS A SOURCE][FACT CHECK THIS]

350 The frequency of light emitted due to cherenkov radiation follows the equation:

$$INSERTCherenkovwavelengthcalcHERE. \quad (3.1)$$

351 The absorption spectra is shown in the following figure:

352 **3.3 Photons ( $\gamma$ )**

353 **3.4 Neutrinos ( $\nu$ )**

354 **3.5 Opportunities to Combine for Dark Matter**



Figure 3.2 TODO: absorption spectrum of liquid and solid water[NEEDS A SOURCE][FACT CHECK THIS]

## CHAPTER 4

355

### HIGH ALTITUDE WATER CHERENKOV (HAWC) OBSERVATORY

356 **4.1 The Detector**

357 **4.2 Events Reconstruction and Data Acquisition**

358 **4.2.1 G/H Discrimination**

359 **4.2.2 Angle**

360 **4.2.3 Energy**

361 **4.3 Remote Monitoring**

362 **4.3.1 ATHENA Database**

363 **4.3.2 HOMER**

364

## CHAPTER 5

### ICECUBE NEUTRINO OBSERVATORY

365 **5.1 The Detector**

366 **5.2 Events Reconstruction and Data Acquisition**

367 **5.2.1 Angle**

368 **5.2.2 Energy**

369 **5.3 Northern Test Site**

370 **5.3.1 PIgeon remote dark rate testing**

371 **5.3.2 Bulkhead Construction**

## CHAPTER 6

### COMPUTATIONAL TECHNIQUES IN PARTICLE ASTROPHYSICS

373 **6.1 Neural Networks for Gamma/Hadron Separation**

374 **6.2 Parallel Computing for Dark Matter Analyses**

375

## CHAPTER 7

### GLORY DUCK

376 **7.1 Dataset and Background**377 **7.1.1 Data Files**

- 378 • Detector Resolution: `response_aerie_svn_27754_systematics_best_mc_test_no`  
 379       `broadpulse\_10pctlogchargesmearing_0.63qe_25kHzNoise_run5481_curvatu`  
 380       `re0_index3.root`
- 381 • Data Map: `maps-20180119/liff/maptree_1024.root`

382 **7.1.2 Data Set Chosen**

383       The maps used for this analysis contain 1017 days of data between runs 2104 (2014-11-26) and  
 384      7476 (2017-12-20). They were generated from pass 4.0 reconstruction. The analysis is performed  
 385      using the  $f_{hit}$  energy binning scheme with bins [1-9] similar to what was done for the Crab and  
 386      previous HAWC dSph analysis. [25, 26].

387 **7.1.3 Background Estimation**

388       This analysis was done on dwarf spheroidal (dSph) galaxies because of their large dark matter  
 389      (DM) content relative to baryonic. We consider the following to estimate the background to this  
 390      study.

- 391       • The dSphs are small in HAWC’s field of view, so the analysis is not sensitive to large or small  
 392       scale anisotropies.
- 393       • The dSphs used in this analysis are off the galactic plane.
- 394       • The dSphs are baryonically faint relative to their expected dark matter content and are not  
 395       expected to contain gamma-ray sources.

396       Therefor we make no additional assumptions of the background coming from our sources and  
 397      use HAWC’s standard direct integration method for background estimation. It is possible for gamma

398 rays from DM annihilation to scatter in transit to HAWC via Inverse Compton Scattering (ICS).  
399 This was investigated and its impact on the flux is basically zero. Supporting information on this  
400 is in **TODO: refer to appdx**

401 **7.1.4 Software Tools and Development**

402 This analysis was performed using HAL and 3ML, in Python version 2.[25, 27] Dan developed  
403 a source model to implement the *Poor Particle Physicists' Cookbook* (PPPC) [28] into HAWC  
404 software. This model and corresponding Monte Carlo simulation was consolidated into a dictionary  
405 for other collaborators. A NumPy version of this dictionary was made for both Py2 and Py3. The  
406 code base for creating this dictionary is also in Dan's sandbox:

- 407 • Py2: <https://gitlab.com/hawc-observatory/sandboxes/salaza82/glory-duc>  
408 k-hawc/-/tree/master/GD\_spectrumDictionary Generator (Deprecated)
- 409 • Py3: <https://gitlab.com/hawc-observatory/sandboxes/salaza82/pppc2dict>  
410 tPPPC2Dict

411 The analysis was performed using the  $f_{\text{hit}}$  framework performed in the Crab paper[25]. The  
412 PPPC model selected for this analysis included electroweak corrections. Dictionaries for the  
413 non-electroweak model were generated but not used for this analysis. The Python2 NumPy dictio-  
414 nary file for gamma-ray final states is `dmCirSpecDict.npy`. The corresponding Python3 file is  
415 `DM_CirrelliSpectrum_dict_gammas.npy`. These files can also be used for decay channels and  
416 the PPPC describes how. [28]. Python's pickle is not backwards compatible, so scripts run in Py3  
417 are not able to use dictionaries generated using Py2 and vice-versa.

418 All other software used for data analysis, DM profile generation, and job submission to SLURM  
419 are also kept in my sandbox for <https://gitlab.com/hawc-observatory/sandboxes/sal>  
420 aza82/glory-duck-hawc the Glory Duck project. They're broad descriptions are as follows:

- 421 • `GD_mass_profiles`: scripts that generate .fits maps for HAWC HAL according to [29].  
422 Also contains simple plots of these maps.

- 423     • `GD_spectrum`: scripts that generate NumPy dictionaries of PPPC gamma spectra [28].
- 424     • `analysis_scripts`: HAL scripts for performing likelihood computation on HAWC data or  
425       simulation with GD spectra and mass profiles.
- 426     • `pointing`: HAL scripts used to compare the impact of point systematic.
- 427     • `poisson_maps`: scripts for generating and managing poisson trials used for this study.

428 **7.2 Analysis**

429 **7.2.1 Monte Carlo Simulation**

430     The expected differential photon flux from a DM-DM annihilation to standard model particles  
431     over solid angle is described by the familiar equation.

$$\frac{d\Phi_\gamma}{dE_\gamma} = \frac{\langle\sigma v\rangle}{8\pi m_\chi^2} \frac{dN_\gamma}{dE_\gamma} \times \int_{\text{source}} d\Omega \int_{l.o.s} \rho_\chi^2 dl(r, \theta') \quad (7.1)$$

432     Where  $\langle\sigma v\rangle$  is the velocity weighted annihilation cross-section.  $\frac{dN}{dE}$  is the expected differential  
433     number of photons produced at each energy per annihilation.  $M_\chi$  is the rest mass of the supposed  
434     DM particle.  $J$  is the astrophysical J-factor and is defined as

435      $\rho_\chi$  is the DM density. For this value, we import the PPPC with electroweak corrections [28].  
436     The spectrum is implemented as a model script in astromodels for 3ML. The J-factor profiles for  
437     each source is imported from Geringer-Sameth ( $\mathcal{GS}$ ) [30]. Another DM distribution model from  
438     Bonnivard ( $\mathcal{B}$ ) [31] was used for the complete study. However, to save computational time, limits  
439     from  $\mathcal{GS}$  were scaled to  $\mathcal{B}$  instead of each experiment performing a full study a second time. We  
440     create NSIDE 16384 maps of the J-factors for each dSph. These maps are integrated over every  
441     spatial bin and passed to the fitting software. Plots of these maps are provided for each source in  
442     the sandbox directory: `GD_mass_profiles`.

443 **7.2.2 Source Selection and Annihilation Channels**

444     We use many of the dSph presented in our previous dSph DM search [26]. HAWC's sources  
445     for Glory Duck include Boötes I, Coma Berenices, Canes Venatici I + II, Draco, Hercules, Leo

446 I, II, + IV, Segue 1, Sextans, and Ursa Major I + II. A full description of all sources used in  
447 Glory Duck is found in ???. Triangulum II was excluded from the Glory Duck analysis because  
448 of large uncertainties in its J-factor. Ursa Minor was excluded from HAWC’s contribution to the  
449 combination because the source extension model extended Ursa Minor beyond HAWC’s field of  
450 view. Ursa Minor was not expected to contribute significantly to the combined limit, so work was  
451 not invested in a solution to include Ursa Minor.

452 The DM annihilation channels probed for the Glory Duck combination include  $b\bar{b}$ ,  $e\bar{e}$ ,  $\mu\bar{\mu}$ ,  $\tau\bar{\tau}$ ,  $t\bar{t}$ ,  $W^+W^-$ , and  $ZZ$ .  
453 A summary of all sources, with a description of each experiments’ sensitivity to the source, is pro-  
454 vided in ??.

455 margin=2.5cm

Table 7.1 Summary of dSph observations by each experiment used in this work. A ‘-’ indicates the experiment did not observe the dSph for this study. For Fermi-LAT, the exposure at 1 GeV is given. For HAWC,  $|\Delta\theta|$  is the absolute difference between the source declination and HAWC latitude. HAWC is more sensitive to sources with smaller  $|\Delta\theta|$ . For IACTs, we show the zenith angle range, the total exposure, the energy range, the angular radius  $\theta$  of the signal or ON region, the ratio of exposures between the background-control (OFF) and signal (ON) regions ( $\tau$ ), and the significance of gamma-ray excess in standard deviations,  $\sigma$ .

| Source name       | Fermi-LAT                       | HAWC                 | H.E.S.S, MAGIC, VERITAS |            |              |                    |
|-------------------|---------------------------------|----------------------|-------------------------|------------|--------------|--------------------|
|                   | Exposure ( $10^{11}$ s m $^2$ ) | $ \Delta\theta $ (°) | IACT                    | Zenith (°) | Exposure (h) | Energy range (GeV) |
| Boötes I          | 2.6                             | 4.5                  | VERITAS                 | 15 – 30    | 14.0         | 100 – 41000        |
| Canes Venatici I  | 2.9                             | 14.6                 | –                       | –          | –            | –                  |
| Canes Venatici II | 2.9                             | 15.3                 | –                       | –          | –            | –                  |
| Carina            | 3.1                             | –                    | H.E.S.S.                | 27 – 46    | 23.7         | 310 – 70000        |
| 2*Coma Berenices  | 2*2.7                           | 2*4.9                | H.E.S.S.                | 47 – 49    | 11.4         | 550 – 70000        |
|                   |                                 |                      | MAGIC                   | 5 – 37     | 49.5         | 60 – 100000        |
| 2*Draco           | 2*3.8                           | 2*38.1               | MAGIC                   | 29 – 45    | 52.1         | 70 – 100000        |
|                   |                                 |                      | VERITAS                 | 25 – 40    | 49.8         | 120 – 70000        |
| Fornax            | 2.7                             | –                    | H.E.S.S.                | 11 – 25    | 6.8          | 230 – 70000        |
| Hercules          | 2.8                             | 6.3                  | –                       | –          | –            | –                  |
| Leo I             | 2.5                             | 6.7                  | –                       | –          | –            | –                  |
| Leo II            | 2.6                             | 3.1                  | –                       | –          | –            | –                  |
| Leo IV            | 2.4                             | 19.5                 | –                       | –          | –            | –                  |
| Leo V             | 2.4                             | –                    | –                       | –          | –            | –                  |
| Leo T             | 2.6                             | –                    | –                       | –          | –            | –                  |
| Sculptor          | 2.7                             | –                    | H.E.S.S.                | 10 – 46    | 11.8         | 200 – 70000        |
| 2*Segue I         | 2*2.5                           | 2*2.9                | MAGIC                   | 13 – 37    | 158.0        | 60 – 100000        |
|                   |                                 |                      | VERITAS                 | 15 – 35    | 92.0         | 80 – 50000         |
| Segue II          | 2.7                             | –                    | –                       | –          | –            | –                  |
| Sextans           | 2.4                             | 20.6                 | –                       | –          | –            | –                  |
| Ursa Major I      | 3.4                             | 32.9                 | –                       | –          | –            | –                  |
| Ursa Major II     | 4.0                             | 44.1                 | MAGIC                   | 35 – 45    | 94.8         | 120 – 100000       |
| Ursa Minor        | 4.1                             | –                    | VERITAS                 | 35 – 45    | 60.4         | 160 – 93000        |

font=small

Table 7.2 Summary of the relevant properties of the dSphs used in the present work. Column 1 lists the dSphs. Columns 2 and 3 present their heliocentric distance and galactic coordinates, respectively. Columns 4 and 5 report the  $J$ -factors of each source given from the  $\mathcal{GS}$  and  $\mathcal{B}$  independent studies and their estimated  $\pm 1\sigma$  uncertainties. The values  $\log_{10} J$  ( $\mathcal{GS}$  set) correspond to the mean  $J$ -factor values for a source extension truncated at the outermost observed star. The values  $\log_{10} J$  ( $\mathcal{B}$  set) are provided for a source extension at the tidal radius of each dSph. **Bolded sources are within HAWC’s field of view and provided to the Glory Duck analysis.**

| Name                     | Distance<br>(kpc) | $l, b$<br>( $^{\circ}$ ) | $\log_{10} J$ ( $\mathcal{GS}$ set)<br>$\log_{10}(GeV^2 cm^{-5} sr)$ | $\log_{10} J$ ( $\mathcal{B}$ set)<br>$\log_{10}(GeV^2 cm^{-5} sr)$ |
|--------------------------|-------------------|--------------------------|--|---|
| <b>Boötes I</b>          | 66                | 358.08, 69.62            | $18.24^{+0.40}_{-0.37}$  | $18.85^{+1.10}_{-0.61}$   |
| <b>Canes Venatici I</b>  | 218               | 74.31, 79.82             | $17.44^{+0.37}_{-0.28}$  | $17.63^{+0.50}_{-0.20}$   |
| <b>Canes Venatici II</b> | 160               | 113.58, 82.70            | $17.65^{+0.45}_{-0.43}$  | $18.67^{+1.54}_{-0.97}$   |
| Carina                   | 105               | 260.11, -22.22           | $17.92^{+0.19}_{-0.11}$  | $18.02^{+0.36}_{-0.15}$   |
| <b>Coma Berenices</b>    | 44                | 241.89, 83.61            | $19.02^{+0.37}_{-0.41}$  | $20.13^{+1.56}_{-1.08}$   |
| <b>Draco</b>             | 76                | 86.37, 34.72             | $19.05^{+0.22}_{-0.21}$  | $19.42^{+0.92}_{-0.47}$   |
| Fornax                   | 147               | 237.10, -65.65           | $17.84^{+0.11}_{-0.06}$  | $17.85^{+0.11}_{-0.08}$   |
| <b>Hercules</b>          | 132               | 28.73, 36.87             | $16.86^{+0.74}_{-0.68}$  | $17.70^{+1.08}_{-0.73}$   |
| <b>Leo I</b>             | 254               | 225.99, 49.11            | $17.84^{+0.20}_{-0.16}$  | $17.93^{+0.65}_{-0.25}$   |
| <b>Leo II</b>            | 233               | 220.17, 67.23            | $17.97^{+0.20}_{-0.18}$  | $18.11^{+0.71}_{-0.25}$   |
| <b>Leo IV</b>            | 154               | 265.44, 56.51            | $16.32^{+1.06}_{-1.70}$  | $16.36^{+1.44}_{-1.65}$   |
| Leo V                    | 178               | 261.86, 58.54            | $16.37^{+0.94}_{-0.87}$  | $16.30^{+1.33}_{-1.16}$   |
| Leo T                    | 417               | 214.85, 43.66            | $17.11^{+0.44}_{-0.39}$  | $17.67^{+1.01}_{-0.56}$   |
| Sculptor                 | 86                | 287.53, -83.16           | $18.57^{+0.07}_{-0.05}$  | $18.63^{+0.14}_{-0.08}$   |
| <b>Segue I</b>           | 23                | 220.48, 50.43            | $19.36^{+0.32}_{-0.35}$  | $17.52^{+2.54}_{-2.65}$   |
| Segue II                 | 35                | 149.43, -38.14           | $16.21^{+1.06}_{-0.98}$  | $19.50^{+1.82}_{-1.48}$   |
| <b>Sextans</b>           | 86                | 243.50, 42.27            | $17.92^{+0.35}_{-0.29}$  | $18.04^{+0.50}_{-0.28}$   |
| <b>Ursa Major I</b>      | 97                | 159.43, 54.41            | $17.87^{+0.56}_{-0.33}$  | $18.84^{+0.97}_{-0.43}$   |
| <b>Ursa Major II</b>     | 32                | 152.46, 37.44            | $19.42^{+0.44}_{-0.42}$  | $20.60^{+1.46}_{-0.95}$   |
| Ursa Minor               | 76                | 104.97, 44.80            | $18.95^{+0.26}_{-0.18}$  | $19.08^{+0.21}_{-0.13}$   |

## **CHAPTER 8**

### **NU DUCK**

456

## BIBLIOGRAPHY

- 458 [1] Anne M. Green. “Dark matter in astrophysics/cosmology”. In: *SciPost Phys. Lect.*  
 459 *Notes* (2022), p. 37. doi: [10.21468/SciPostPhysLectNotes.37](https://doi.org/10.21468/SciPostPhysLectNotes.37). URL: <https://scipost.org/10.21468/SciPostPhysLectNotes.37>.
- 461 [2] Bing-Lin Young. “A survey of dark matter and related topics in cosmology”. In: *Frontiers*  
 462 *of Physics* 12 (Oct. 2016). doi: <https://doi.org/10.1007/s11467-016-0583-4>.  
 463 URL: <https://doi.org/10.1007/s11467-016-0583-4>.
- 464 [3] Gianfranco Bertone, Dan Hooper, and Joseph Silk. “Particle dark matter: evidence,  
 465 candidates and constraints”. In: *Physics Reports* 405.5 (2005), pp. 279–390. ISSN:  
 466 0370-1573. doi: <https://doi.org/10.1016/j.physrep.2004.08.031>. URL:  
 467 <https://www.sciencedirect.com/science/article/pii/S0370157304003515>.
- 468 [4] Gianfranco Bertone and Dan Hooper. “History of dark matter”. In: *Rev. Mod. Phys.*  
 469 90 (4 Aug. 2018), p. 045002. doi: [10.1103/RevModPhys.90.045002](https://doi.org/10.1103/RevModPhys.90.045002). URL: <https://link.aps.org/doi/10.1103/RevModPhys.90.045002>.
- 471 [5] Fritz Zwicky. “The Redshift of Extragalactic Nebulae”. In: *Helvetica Physica Acta* 6.  
 472 (1933), pp. 110–127. doi: [10.5169/seals-110267](https://doi.org/10.5169/seals-110267).
- 473 [6] Vera C. Rubin and Jr. Ford W. Kent. “Rotation of the Andromeda Nebula from a Spectro-  
 474scopic Survey of Emission Regions”. In: *ApJ* 159 (Feb. 1970), p. 379. doi: [10.1086/150317](https://doi.org/10.1086/150317).
- 476 [7] K. G. Begeman, A. H. Broeils, and R. H. Sanders. “Extended rotation curves of spiral galax-  
 477 ies: dark haloes and modified dynamics”. In: *Monthly Notices of the Royal Astronomical So-*  
 478 *ciety* 249.3 (Apr. 1991), pp. 523–537. ISSN: 0035-8711. doi: [10.1093/mnras/249.3.523](https://doi.org/10.1093/mnras/249.3.523).  
 479 eprint: <https://academic.oup.com/mnras/article-pdf/249/3/523/18160929/mnras249-0523.pdf>. URL: <https://doi.org/10.1093/mnras/249.3.523>.
- 481 [8] *Different types of gravitational lenses*. website. Feb. 2004. URL: <https://esahubble.org/images/heic0404b/>.
- 483 [9] Douglas Clowe et al. “A Direct Empirical Proof of the Existence of Dark Matter”. In: *apjl*  
 484 648.2 (Sept. 2006), pp. L109–L113. doi: [10.1086/508162](https://doi.org/10.1086/508162). arXiv: [astro-ph/0608407](https://arxiv.org/abs/astro-ph/0608407)  
 485 [*astro-ph*].
- 486 [10] Planck Collaboration and N. et. al. Aghanim. “Planck 2018 results I. Overview and the  
 487 cosmological legacy of Planck”. In: *A&A* 641 (2020). doi: [10.1051/0004-6361/201833880](https://doi.org/10.1051/0004-6361/201833880). URL: <https://doi.org/10.1051/0004-6361/201833880>.
- 489 [11] Wayne Hu. *Matter Density Animation*. web. 2024. URL: <http://background.uchicago.edu/~whu/animbut/anim2.html>.

- 491 [12] Wenlong Yuan et al. “A First Look at Cepheids in a Type Ia Supernova Host with JWST”. in:  
492 *The Astrophysical Journal Letters* 940.1 (Nov. 2022). doi: [10.3847/2041-8213/ac9b27](https://doi.org/10.3847/2041-8213/ac9b27).  
493 URL: <https://dx.doi.org/10.3847/2041-8213/ac9b27>.
- 494 [13] Wendy L. Freedman. “Measurements of the Hubble Constant: Tensions in Perspective”. In:  
495 *The Astrophysical Journal* 919.1 (Sept. 2021), p. 16. doi: [10.3847/1538-4357/ac0e95](https://doi.org/10.3847/1538-4357/ac0e95).  
496 URL: <https://dx.doi.org/10.3847/1538-4357/ac0e95>.
- 497 [14] Jodi Cooley. “Dark Matter direct detection of classical WIMPs”. In: *SciPost Phys. Lect.  
498 Notes* (2022), p. 55. doi: [10.21468/SciPostPhysLectNotes.55](https://doi.org/10.21468/SciPostPhysLectNotes.55). URL: <https://scipost.org/10.21468/SciPostPhysLectNotes.55>.
- 500 [15] “Search for new phenomena in events with an energetic jet and missing transverse momentum  
501 in  $pp$  collisions at  $\sqrt{s} = 13$  TeV with the ATLAS detector”. In: *Phys. Rev. D* 103  
502 (11 July 2021), p. 112006. doi: [10.1103/PhysRevD.103.112006](https://doi.org/10.1103/PhysRevD.103.112006). URL: <https://link.aps.org/doi/10.1103/PhysRevD.103.112006>.
- 504 [16] *Jetting into the dark side: a precision search for dark matter*. website. July 2020. URL:  
505 <https://atlas.cern/updates/briefing/precision-search-dark-matter>.
- 506 [17] Celine Armand et. al. “Combined dark matter searches towards dwarf spheroidal galaxies  
507 with Fermi-LAT, HAWC, H.E.S.S., MAGIC, and VERITAS”. in: *Proceedings of Science*.  
508 Vol. 395. Mar. 2022. doi: <https://doi.org/10.22323/1.395.0528>.
- 509 [18] Tracy R. Slatyer. “Les Houches Lectures on Indirect Detection of Dark Matter”. In: *SciPost  
510 Phys. Lect. Notes* (2022), p. 53. doi: [10.21468/SciPostPhysLectNotes.53](https://doi.org/10.21468/SciPostPhysLectNotes.53). URL:  
511 <https://scipost.org/10.21468/SciPostPhysLectNotes.53>.
- 512 [19] Christian W Bauer, Nicholas L. Rodd, and Bryan R. Webber. “Dark matter spectra from  
513 the electroweak to the Planck scale”. In: *Journal of High Energy Physics* 2021.1029-8479  
514 (June 2021). doi: [https://doi.org/10.1007/JHEP06\(2021\)121](https://doi.org/10.1007/JHEP06(2021)121).
- 515 [20] Riccardo Catena and Piero Ullio. “A novel determination of the local dark matter density”.  
516 In: *Journal of Cosmology and Astroparticle Physics* 2010.08 (Aug. 2010), p. 004. doi:  
517 [10.1088/1475-7516/2010/08/004](https://doi.org/10.1088/1475-7516/2010/08/004). URL: <https://dx.doi.org/10.1088/1475-7516/2010/08/004>.
- 519 [21] B. P. Abbott et al. “Observation of Gravitational Waves from a Binary Black Hole Merger”.  
520 In: *Phys. Rev. Lett.* 116 (6 Feb. 2016), p. 061102. doi: [10.1103/PhysRevLett.116.061102](https://doi.org/10.1103/PhysRevLett.116.061102). URL: <https://link.aps.org/doi/10.1103/PhysRevLett.116.061102>.
- 522 [22] R. Abbasi et. al. “Observation of high-energy neutrinos from the Galactic plane”. In: *Science*  
523 380.6652 (June 2023), pp. 1338–1343.
- 524 [23] NASA Goddard Space Flight Center. *Fermi’s 12-year view of the gamma-ray sky*. website.

- 525 2022. URL: <https://svs.gsfc.nasa.gov/14090>.
- 526 [24] Marco Cirelli et al. “PPPC 4 DM ID: a poor particle physicist cookbook for dark matter  
527 indirect detection”. In: *Journal of Cosmology and Astroparticle Physics* 2011.03 (Mar.  
528 2011), p. 051. doi: [10.1088/1475-7516/2011/03/051](https://dx.doi.org/10.1088/1475-7516/2011/03/051). URL: <https://dx.doi.org/10.1088/1475-7516/2011/03/051>.
- 530 [25] A. U. Abeysekara et al. “Observation of the Crab Nebula with the HAWC Gamma-Ray  
531 Observatory”. In: *The Astrophysical Journal* 843.1 (June 2017), p. 39. doi: [10.3847/1538-4357/aa7555](https://doi.org/10.3847/1538-4357/aa7555). URL: <https://doi.org/10.3847/1538-4357/aa7555>.
- 533 [26] A. Albert et al. “Dark Matter Limits from Dwarf Spheroidal Galaxies with the HAWC  
534 Gamma-Ray Observatory”. In: *The Astrophysical Journal* 853.2 (Feb. 2018), p. 154. ISSN:  
535 1538-4357. doi: [10.3847/1538-4357/aaa6d8](https://dx.doi.org/10.3847/1538-4357/aaa6d8). URL: [http://dx.doi.org/10.3847/1538-4357/aaa6d8](https://dx.doi.org/10.3847/1538-4357/aaa6d8).
- 537 [27] Giacomo Vianello et al. *The Multi-Mission Maximum Likelihood framework (3ML)*. 2015.  
538 arXiv: [1507.08343](https://arxiv.org/abs/1507.08343) [astro-ph.HE].
- 539 [28] Marco Cirelli et al. “PPPC 4 DM ID: a poor particle physicist cookbook for dark matter  
540 indirect detection”. In: *Journal of Cosmology and Astroparticle Physics* 2011.03 (Mar.  
541 2011). ISSN: 1475-7516. doi: [10.1088/1475-7516/2011/03/051](https://dx.doi.org/10.1088/1475-7516/2011/03/051). URL: [http://dx.doi.org/10.1088/1475-7516/2011/03/051](https://dx.doi.org/10.1088/1475-7516/2011/03/051).
- 543 [29] Alex Geringer-Sameth, Savvas M. Koushiappas, and Matthew Walker. “Dwarf galaxy  
544 annihilation and decay emission profiles for dark matter experiments”. In: *Astrophys.  
545 J.* 801.2 (2015), p. 74. doi: [10.1088/0004-637X/801/2/74](https://dx.doi.org/10.1088/0004-637X/801/2/74). arXiv: [1408.0002](https://arxiv.org/abs/1408.0002)  
546 [astro-ph.CO].
- 547 [30] Alex Geringer-Sameth, Savvas M. Koushiappas, and Matthew Walker. “DWARF GALAXY  
548 ANNIHILATION AND DECAY EMISSION PROFILES FOR DARK MATTER EXPERI-  
549 MENTS”. in: *The Astrophysical Journal* 801.2 (Mar. 2015), p. 74. ISSN: 1538-4357. doi:  
550 [10.1088/0004-637x/801/2/74](https://dx.doi.org/10.1088/0004-637x/801/2/74). URL: [http://dx.doi.org/10.1088/0004-637X/801/2/74](https://dx.doi.org/10.1088/0004-637X/801/2/74).
- 552 [31] V. Bonnivard et al. “Spherical Jeans analysis for dark matter indirect detection in dwarf  
553 spheroidal galaxies - Impact of physical parameters and triaxiality”. In: *Mon. Not. Roy.  
554 Astron. Soc.* 446 (2015), pp. 3002–3021. doi: [10.1093/mnras/stu2296](https://doi.org/10.1093/mnras/stu2296). arXiv:  
555 [1407.7822](https://arxiv.org/abs/1407.7822) [astro-ph.HE].